frontiers in Physics

REVIEW
published: 14 August 2020
doi: 10.3389/fphy.2020.00312

One-Dimensional Plasmonic Sensors

Yitian Liu [1,2] *and Yaoguang Ma* [1,2]*

[1] State Key Laboratory of Modern Optical Instrumentation, Zhejiang University, Hangzhou, China, [2] College of Optical Science and Engineering, Zhejiang University, Hangzhou, China

Recent advances in surface plasmon sensors have significantly reduced the limitations of conventional optical sensors. With the recent development of micro- and nano-fabrication technology, miniaturized one-dimensional structures become a promising platform for surface plasmon sensors for its compactness and simple structure. In this review, we describe the generation of surface plasmon polaritons and the resonance conditions. Then we categorize surface plasmon sensors by the physical quantities they detect, elaborating their working principle, performance, and current development. Finally, we summarize both limitations and advances of various design methods to provide an outlook on future directions of this field.

Keywords: surface plasmon resonance, localized surface plasmon resonance, biochemical sensing, refractive index, waveguide, nanowires

OPEN ACCESS

Edited by:
Lin Chen,
University of Shanghai for Science and Technology, China

Reviewed by:
Ilia L. Rasskazov,
University of Rochester, United States
Junichi Fujikata,
Photonics Electronics Technology Research Association, Japan

***Correspondence:**
Yaoguang Ma
mayaoguang@zju.edu.cn

Specialty section:
This article was submitted to Optics and Photonics, a section of the journal Frontiers in Physics

Received: *04 April 2020*
Accepted: *07 July 2020*
Published: *14 August 2020*

Citation:
Liu Y and Ma Y (2020) One-Dimensional Plasmonic Sensors. Front. Phys. 8:312. doi: 10.3389/fphy.2020.00312

INTRODUCTION

Optical sensors are used for a broad range of applications, ranging from simple distance detection to providing artificial vision for object recognition. One of the critical challenges that modern sensor industry faces are to explore novel nanostructures with designer functions. Among the other nanotechnologies, the idea of utilizing surface plasmon polaritons (SPPs) proves itself useful over other competitors. Metallic nanostructures are promising for the generation and distribution of electromagnetic radiation in unprecedented ways. SPPs, also known in the literature as surface plasma waves (SPWs) [1], are coherent oscillations of free electrons at the interface between metal and dielectric [2]. They possess a series of novel optical properties, such as local electric field enhancement, deep subwavelength confinement of optical fields, etc. The highly confined electromagnetic field could break the optical diffraction limit, making SPP-based sensors exhibit high sensitivity and miniaturized size [3]. Also, the high energy density in the near field of SPPs contributes significantly to the sensor sensitivity for special applications, such as single molecular sensing. Compared to conventional techniques, such as fluorescence analysis, SPP-based sensors are more compatible with analyte and does not involve additional processes like labeling. And the application of SPPs has gained tremendous attention in optical sensing areas since its first gas sensing demonstration [4].

In the visible and infrared region, SPPs can be supported by one-dimensional structures. However, the electromagnetic characteristics of metals in the terahertz band are similar to perfect electrical conductors (PEC), and cannot support SPPs for practical applications [5]. Therefore, pleated subwavelength structures with different geometric features can support spoof SPPs in the terahertz band for sensing applications [6, 7]. Compared with these structures, one-dimensional waveguide structure has properties, such as mass production and low cost. Furthermore, one-dimensional structures are important for the integrated plasmonic circuit, which have attracted increasing attentions for flexible and compact applications in optical sensors [8–10]. Additionally, one-dimensional waveguide structure can guide SPPs along metal-dielectric interfaces beyond the diffraction limit and confine light to scales $< \lambda/10$ along relatively long distance [11], thus high sensitivity can be achieved in one-dimensional sensors.

In recent years, boosted by the dramatic progress made in micro- and nano-fabrication technology [12–14] these years, plasmonic sensors have demonstrated their advantages in various areas, such as chemical sensing [15–17], biological species [18, 19], environmental monitoring [20, 21], food safety [22–24], and medical diagnosis [8, 25–27]. Notably, these sensors offer distinguishing characteristics in biochemical analyses [28, 29]. Recently, an SPP-based test paper for rapid detection of COVID-19 has been released in Japan [30]. Antibiotic coated gold nanoparticles that undergo resonance peak shift show a distinct color change when COVID-19 viruses are captured. Similar methods are widely applied in pregnancy test.

In this review, we start with a brief introduction of the concept of SPPs at the interface of metal and dielectric interface, followed by a description of excitation and coupling schemes used for one-dimensional waveguiding structures. Then we give a short discussion on the distinction between localized surface plasmon polariton (LSPP) for small nanoparticles (NPs) and SPP in elongated nanostructures, such as metallic nanowires (NWs). In the third part, some critical applications for 1-D waveguide are presented, and these include a refractive index, pressure, and biochemical sensing. These demonstrations underline the advantages 1-D nanostructures bring to the nanoscience and nanotechnology field. Finally, we summarize the possible future developments of 1-D waveguide sensors, such as metallic nanowires, etc., in various research areas.

PHYSICS OF SURFACE PLASMONS

Optical Excitation of Surface Plasmon Polaritons

To describe these peculiar behaviors of SPPs, we start from the description of the motion of a free electron in metal:

$$m\frac{d^2x}{dt^2} + m\gamma\frac{dx}{dt} = -eE_0\exp(-i\omega t) \tag{1}$$

where x is the displacement of the electron, m is the electron mass, γ is the damping factor, e is the charge of an electron, E_0 is the amplitude of the external electric field, and ω is the angular frequency of the external electric field. By solving Equation (1), we get the Drude model of free electrons in metal as:

$$\varepsilon(\omega) = \varepsilon_r + i\varepsilon_i = 1 - \frac{{\omega_p}^2}{\omega(\omega+i\gamma)} \tag{2}$$

where ω_p stands for the plasma frequency. We assume $\gamma \ll \omega_p$ and then obtain the relation between the dielectric constant of metal and the frequency of the incident light.

SPPs are longitudinal waves propagating along an interface as shown in **Figure 1A**. The confinement is achieved due to the fact that the wave vector of SPPs is much larger than that of light wave in the dielectric. The wave vector of SPPs propagating along the metal surface is given by

$$k_{SPP} = \frac{\omega}{c}\sqrt{\frac{\varepsilon(\omega)\varepsilon_m}{\varepsilon(\omega)+\varepsilon_m}} \tag{3}$$

where ω is the angular frequency, c is the speed of light in vacuum, $\varepsilon(\omega)$, and ε_m are the dielectric constants of the dielectric and metal, respectively.

For a given wavelength, the light line always lies to the left of the SPP dispersion curve as shown in **Figure 1B**. The phase-matching condition therefore forbids a direct coupling between 3-dimensional light and 2-dimensional SPP. Various techniques utilizing prisms, gratings, highly focused beam, and optical nanofibers, etc., have been proposed to address this issue.

SPPs undergoes severe attenuation in the metal film layer, which decreases the intensity of the electromagnetic field. The propagation length of SPPs is defined as:

$$L = \frac{1}{2Im\{k_{spp}\}} \tag{4}$$

L typically ranges from 10 to 100 μm in the visible regime [31]. It limits the maximum size of SPP-based devices to ensure that the attenuation of energy is reasonable. The propagation length and penetration depth are both dependent on frequency. For frequencies close to the surface plasma frequency, SPPs exhibit strong field confinement to the interface and a short propagation distance at the same time, which is a trade-off between energy confinement and loss for SPP-based devices.

The penetration depth is defined to represent the distance from the interface when the amplitude of SPPs decays by a factor of $1/e$. According to the z component of wave vector in the metal layer and that in the dielectric layer solved by Maxwell's equation, the penetration depth is:

$$L_p = \frac{1}{Re\{k_z\}} \tag{5}$$

where $k_z = \sqrt{{k_{spp}}^2 - \varepsilon_i\left(\frac{\omega}{c}\right)^2}$, ε_i refers to ε_m in the metal layer and ε_d in the dielectric layer. In most cases, SPPs penetrate deeper into the dielectric layer than that in the metal layer, as indicated in **Figure 1A**. In SPP-based sensors, the penetration depth in the dielectric layer determines the actual sensing area.

Optical Excitation of Localized Surface Plasmon Polaritons

As is shown in **Figure 1C**, in contrast to SPPs that propagate along continuous metal surfaces, LSPPs are non-propagating excitations tightly confined to the nanostructure. Conduction electrons in the NPs oscillate collectively and locally with a resonant frequency, which depends upon the composition, size, geometry, dielectric environment, and particle-to-particle separation of NPs [32]. The excitation of LSPR gives rise to field enhancement of local electromagnetic fields on the surface of an NP or "hot spots" between NPs, and results in strong scattering and the absorption of the incident light. LSPP shows more significant potential for sensing analytes with small concentrations and provides an approach in surface plasmon-enhanced sensing.

Here we can use the quasi-static approximation (**Figure 1D**) since the radius of an NP is much smaller than the wavelength of

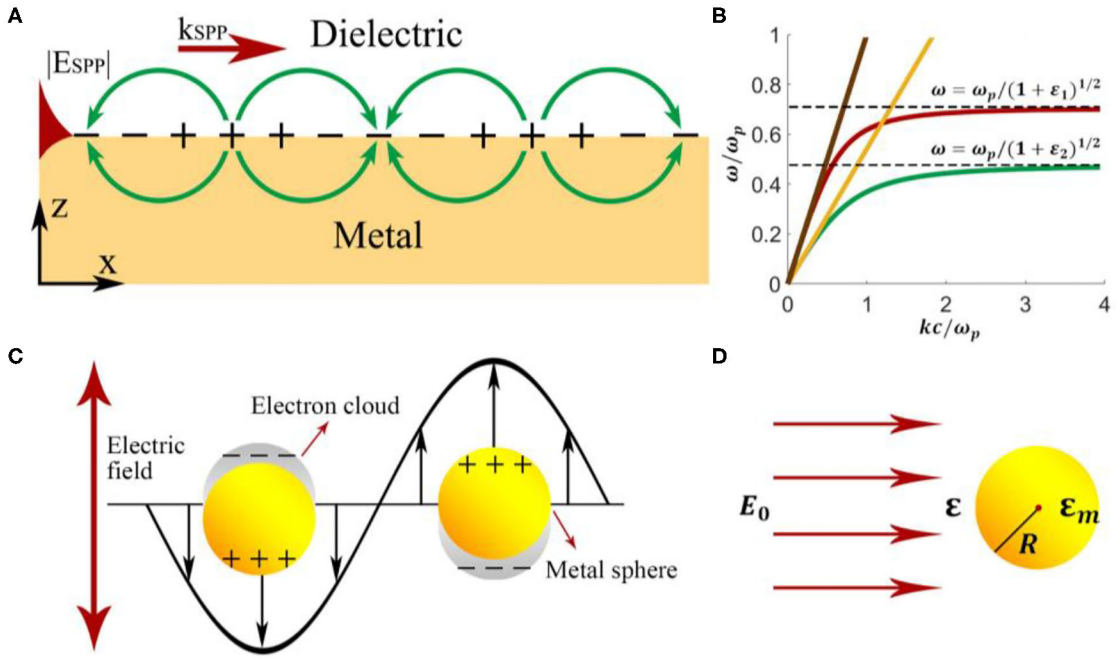

FIGURE 1 | Schematic illustration of **(A)** surface plasmon polaritons and **(B)** excitation of SPPs on the metal-vacuum interface. The two curves are the dispersion relation of SPPs on the metal-vacuum interface (red line) and that on the metal-GaAs interface (green line). The dispersion relations of light incident from vacuum and GaAs are plotted as the yellow line and the brown line, respectively. **(C)** Localized surface plasmon polaritons at the interface between metal nanoparticles and dielectric environment. **(D)** A metal nanoparticle with a radius R in the electric field E_0.

the incident light. According to the boundary conditions and the dipole model, the polarizability of the particle can be written as

$$\alpha = 4\pi R^3 \frac{\varepsilon - \varepsilon_m}{\varepsilon + 2\varepsilon_m} \tag{6}$$

where ε and ε_m are the dielectric constant of the spherical particle and that of the environment, respectively. Further deduction gives the absorption cross-section and the scattering cross-section of the particle as

$$C_{abs} = kIm\{\alpha\} = 4k\pi R^3 Im\left\{\frac{\varepsilon - \varepsilon_m}{\varepsilon + 2\varepsilon_m}\right\} \tag{7}$$

$$C_{scat} = \frac{k^4}{6\pi}|\alpha|^2 = \frac{8}{3}k^4\pi R^6\left|\frac{\varepsilon - \varepsilon_m}{\varepsilon + 2\varepsilon_m}\right|^2 \tag{8}$$

As is shown in Equations (7) and (8), the scattering cross-section and the absorption cross-section is proportional to the 6th power and 3rd power of the radius, respectively. That is, light scattering accounts for the main contribution for relatively large particles, and for small particles, the proportion of light absorption is more substantial. The quasi-static model used here treats plasmonic particles as dipoles and neglects the delay effect as well as the damping effect. However, larger particles, especially particles with the diameter comparable to the wavelength, cannot be considered as dipoles. Higher-order modes must be taken into account when dealing with these problems. The sensible polarizability of metallic particles is calculated by the modified long-wavelength approximation model (MLWA) [3], which explains perfectly why the redshift of the LSPR peak position as the size of NPs increase, is a more sensible solution for polarizability of large metallic particles.

PERFORMANCE EVALUATION OF SURFACE PLASMON SENSORS

The principle of SPP sensing is based on the change of the SPP's spectra or intensity upon the change of environment. The first parameter we would take into account when designing a sensor is the sensitivity (S). It is determined by the ratio of the change in sensor output to the difference in the measured parameter. In the SPP-based sensors, the quantity measured is generally the refractive index (n), and the output quantity (Y), which could be the resonant angle, resonant wavelength, intensity of guided waves, and phase shift.

$$S = \frac{dY}{dn} \tag{9}$$

According to Equation (9), the sensitivity of intensity interrogation can be expressed in the unit of RIU^{-1} (*RIU* for Refractive Index Unit). In SPP sensors with wavelength modulation, the sensor output is the coupling wavelength and the sensitivity unit is usually μm/RIU or nm/RIU, which indicates the spectra position shifts vs. the change of analyte's RI. Moreover, the sensitivity of angular or phase modulation sensors is described in terms of rad/RIU or deg/RIU. By detecting the

propagation constant differences, researchers can also achieve sensitivity in the form of rad/(μm·RIU).

Usually, sensitivity takes the global RI into account in physical sensing approaches. But the sensitivity of an SPP-based sensor only considers the RI changes in a local region, as electromagnetic field is confined tightly near the interface of metallic nanostructures, for example, the local RI difference caused by biomacromolecules. It's worth noting that, in LSPP-based biochemical sensors, the distribution of the electromagnetic field is not uniform on the surface of NPs. Generally, the electric field is distributed at locations with small curvature radius, tips, and gaps. Thus, it is essential to attach molecules to these local areas when designing the sensor to enhance sensitivity.

Resolution, or detection limit (*DL*), is another important parameter which is adjusted by the smallest variation in the environmental refractive index that can be detected by the sensor [33]. The noise of the output signal (σ) and the sensitivity of the sensor (S) determines it together. Therefore, sensors can exhibit high resolution by improving their signal-to-noise ratio or sensitivity.

$$DL = \frac{\sigma}{S} \tag{10}$$

Aside from the above-mentioned parameters, linearity and dynamic ranges are crucial evaluation parameters that describe the stability of SPP-based sensors. The linearity indicates the ratio of the sensor output to the parameter measurement and represents the sensor's stability during the detection process. A high linearity response of the regression line indicates an excellent sensor [34]. The dynamic range describes the span of the values of the measurand that can be measured by the sensor [35]. As for the refractive index sensors, dynamic range refers to the variety refractive index that sensors can measure under specific accuracy.

SURFACE PLASMON SENSORS BASED ON ONE-DIMENSIONAL WAVEGUIDE

Recent waveguide-based surface plasmon sensors can be categorized based on the physical quantities they measure. Moreover, to achieve high sensitivity and compactness simultaneously, one-dimensional waveguide structures, such as an integrated waveguide, optical fibers, and nanowires are mainly discussed.

Refractive Index Sensors

Since the invention of the first SPP-based sensor for gas detection [4], these sensors based on Otto structure and Kretschmann structure have been widely used in the fields of physical, chemical, and biological measurements. The refractive index alters when changes in these measured quantities take place. However, the conventional prism SPP-based sensor has bulky optical and mechanical components and has no advantages in integrated applications.

Optical Fiber-Based RI Sensors

Optical fiber based SPP sensors provide a favorable choice for miniaturized sensing and are incredibly suitable for *in vivo* applications. In 1993, Jorgenson et al. [15] proposed the first optical fiber-based SPP configuration without the bulk light coupling prism. By partially removing the fiber cladding and depositing a high reflective layer at the exposed position, a fiber-based SPP refractive index sensor was proposed utilizing the interaction of evanescent waves with SPPs.

Scientists proposed several approaches [36–38] to enhance the sensitivity of fiber-based SPP sensors. Monzón-Hernández et al. [37] deposited a thin metal layer on a single-mode tapered optical fiber, so the fundamental fiber mode can excite different surface plasmon modes to acquire multiple resonance peaks. The fiber-based sensor achieves a RI resolution of 7×10^{-7} RIU when monitoring the three most profound peaks. Gupta et al. [38] proposed a fiber-based SPP probe consists of a fiber core, silver layer, silicon layer, and sensing medium. This SPP sensor has shown a sensitivity increasing from 2.8452 to 5.1994 μm/RIU when employing a 10-nm-thick silicon layer. Additionally, this silicon layer can prevent the plasmonic layer from oxidation and help tune the resonance. Although optical fiber-based SPP sensors possess the advantages of miniaturization and high sensitivity, their sensing range is usually limited. And the necessary for a spectrometer with an expensive and bulk size makes it challenging to realize the low cost and compact of the overall system.

Integrated Waveguide-Based RI Sensors

Integrated waveguide SPP sensors are particularly promising in the development of miniaturized multi-channel on-chip sensing devices. Suzuki et al. [39] proposed a sensing system with dual LEDs and monitored the differential signal by photodiodes. This system is low-priced and compact since dual LEDs and photodiodes can replace laser and spectrometer, respectively.

The silicon-on-insulator (SOI) rib waveguide with a large cross-section has the characteristics of low transmission loss and integratable with optical fiber communication systems [40]. Yuan et al. proposed an SOI rib waveguide-based sensor by coupling light from single-mode fibers to various units of the SOI rib waveguide array [40]. The analyte refractive index are calculated from the shift of the reflection spectrum. Although the refractive index detection limit is higher (5.3×10^{-5} RIU) comparing with a single SPP sensor (5.04×10^{-7} RIU), it is more cost-effective and compact. Imprinting techniques that help fabricate these sensors with high throughput speed further lows the cost [41]. Using this fabrication method, Matsushita et al. fabricated polymer sensor chips with a refractive index resolution of 3.8×10^{-4} RIU and a noise fluctuation of ∼1.2%.

Compared with sensors based on the intensity-detection method, SPP interferometry shows a resolution orders of magnitude higher [42, 43]. Mach-Zenhnder interferometer (MZI) based sensors are useful for restricted refractive index measurements, such as in fluid-based biological detection. Sheridan et al. build a model describing the dependency of MZI transmittance as a function of substrate index. Their model indicates that an increase in the refractive index sensitivity can

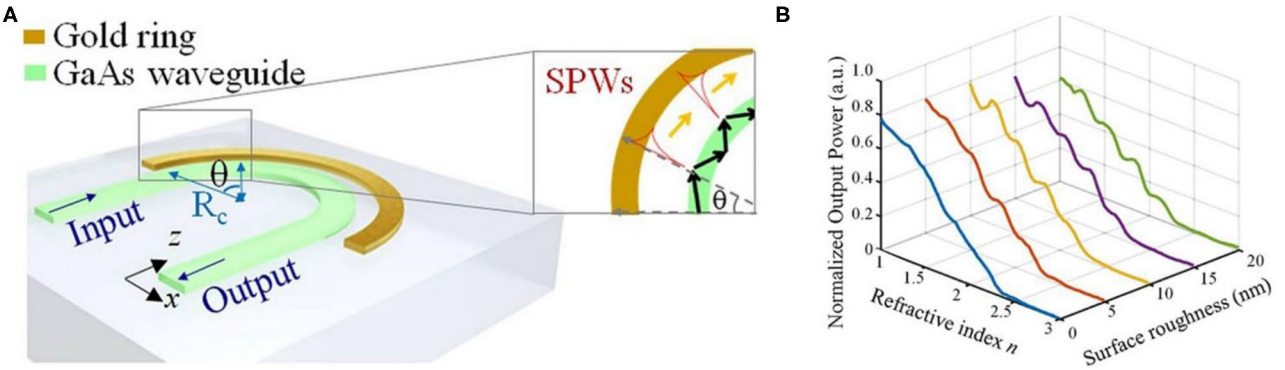

FIGURE 2 | Schematic and performance of a curved-waveguide-based SPP sensor [46]. **(A)** Schematic of a curved-waveguide-based SPP sensor. The configuration contains a curved GaAs waveguide surrounding by an outer gold ring. The inset picture shows multiple SPW excitations along the surface of the gold ring. **(B)** The performance of normalized output power vs. refractive index for different surface roughness σ ranging from 0 to 20 nm. Reprinted with permission from Cheng et al. [46] © Springer Nature.

be achieved compared to conventional waveguide SPP sensors when a phase bias is applied in one branch [44]. Based on MZI structure, Nemova et al. [45] explored a sensor tool with the phase Bragg grating imprinted in one branch, which serves for excitation of SPPs. The reported refractive index resolution is 3×10^{-7} RIU. However, the dynamic range is reduced by approximately two orders of magnitude compared to the intensity measuring sensor. Additionally, interferometry configuration can partially suppress unwanted refractive index changes act on both branches, like temperature or pressure variations. Cheng et al. [46] proposed a novel SPP sensor with an extensive dynamic range, high sensitivity, and compact structure numerically. This sensor includes a GaAs curved waveguide surrounding by an outer gold ring waveguide, as shown in **Figure 2A** [46]. Since the evanescent field changes with the background refractive index, the background refractive index can be obtained by measuring the output power of the waveguide. In **Figure 2B** [46], high linearity is achieved in the dynamic range of $n = 1$–2.36, considering the surface roughness of $\sigma = 5$ nm. The numerical resolution is as high as 4.53×10^{-10} RIU and is the same for both gas and liquid situations.

Biochemical Sensors

SPP biosensors are the primary technology used to study macromolecules and their functions in life science and medical research. Also, SPP biosensors can be implemented in pollutant detection, social health indicators detection, and food toxin detection. SPP biosensors are composed of an SPP sensor and a suitable bio-recognition element. The sensor tracks the refractive index change around the surface when bio-interactions take place, thus providing us the bio-information as designed.

Noble Metal Nanowire Based SPP Biochemical Sensors

Noble metal NW naturally acts as one-dimensional optical waveguide [47]. Despite its miniaturized footprint, NWs can confine light field tightly around the metal interface and to produce confinement beyond the diffraction limit. NWs have become a novel candidate for biochemical sensing in recent years since they are highly sensitive and are observable under an optical microscope [48].

Focusing light with parallel polarization onto the end of a NW could excite SPPs propagating in the NW. Here, **Figure 3A** [49] shows a structure of an NW sensor demonstrated by Wei et al. The structure consists of Ag NWs deposited on a glass substrate, coated with Al_2O_3 layers of different thickness T. The quantum dots (QDs) act as a local field reporter to give the image of near-field distributions near NWs. QD fluorescence captured by camera reveals the plasmon beating period (Λ) increases with the dielectric (Al_2O_3) thickness T dramatically. Λ increases from ∼1.7 μm (top) to 5.8 μm (bottom) with T changes from 30 to 80 nm. The NW plasmonic sensor detects the last mode position change of ∼360 nm per nanometer of Al_2O_3 coating, and the sensitivity can be further improved by enlarging for longer wires and more period.

Another approach uses the transmission spectra collected from the NW sensor. Gu et al. from Zhejiang University demonstrate a single-nanowire plasmonic sensor for hydrogen and humidity sensing [20]. During the sensing process, light is coupled from a silica fiber taper to the NWs and is collected by another fiber taper. For hydrogen sensing, using Pd-coated Au NW with an 80 nm diameter and a 25 μm length, an intensity change of ∼13 dB is achieved as the hydrogen concentration varied from 0 to 1.2%. For humidity sensing, polyacrylamide film-supported Ag NW is employed to achieve response time of 5 ms when relative humidity jumps from 82 to 70%, for its small interaction area and short length.

An NW-assembled MZI has been proposed by Wang et al. [50]. Two Au NWs and two fiber tapers forms the MZI by delicate micro manipulation. One NW is immersed in the measured liquid while the other is used as a reference. Based on the MZI structure, the molar concentration of benzene can be measured by detecting the propagation constant differences, achieving a sensitivity of 5.5π/(μm·RIU) with 660-nm-wavelength probing

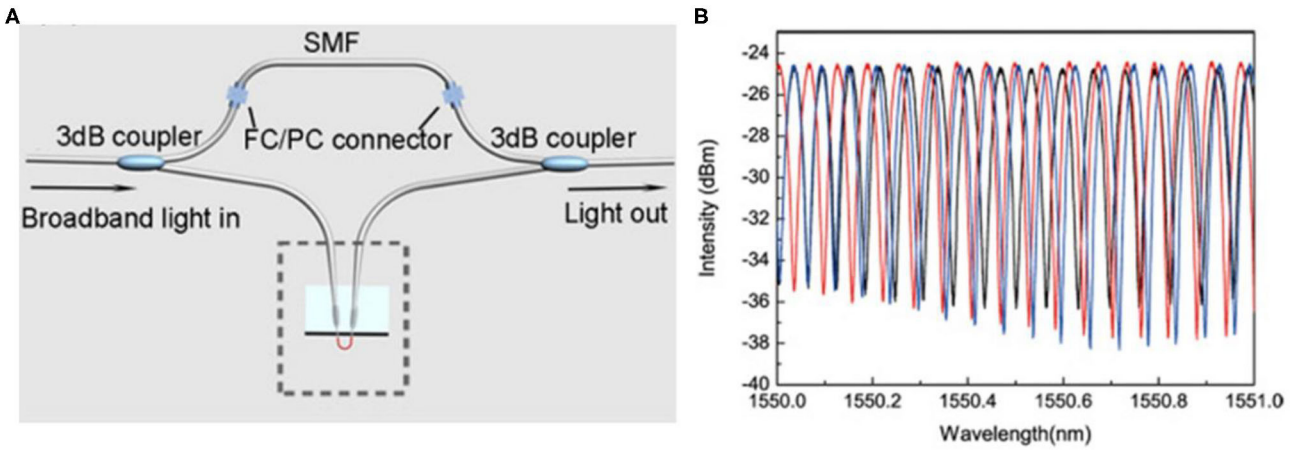

FIGURE 3 | Schematic and performance of an NW-assembled MZI sensor [17]. **(A)** All-fiber hybrid photonic-plasmonic MZI. **(B)** Spectral shifts of the interference peak when the probe is exposed to NH3 of 80 ppm (blue) and 160 ppm (red), respectively. Reprinted with permission from Li et al. [17] © The Optical Society.

light propagating in a 100-nm-diameter Au NW. The MZI sensor proposed by Li et al. is schematically illustrated in **Figure 3A** [17]. Two commercial Y-couplers are connected and an NW-assembled fiber-based plasmonic probe is inserted in one arm. **Figure 3B** [17] shows the spectral shift of the interference fringes when the probe is exposed to ammonia gas (NH_3) of 80 and 160 ppm. This sensor shows a detection limit lower than 80 ppm for NH_3 and a response time of 400 ms (rising time) and 300 ms (falling time).

Nanoparticle-Nanowire Hybrid Nanostructures Based Biochemical Sensors

SiO_x NW-Au NP composites have shown interesting plasmonic properties. Wang et al. [51] utilized a single gold-peapodded silica NWs structure and proposed a photo-enhanced oxygen sensing method. Compared to the bare SiO_2 NWs, Au-NP@SiO_2 NWs exhibit a significantly stronger LSPP-enhanced E field around the Au NPs surface for both TE and TM mode. The induced absorption originated from LSPR in NPs provides improved response and 750 s faster recovery time compared to bare SiO_2 NWs. A systematic and quantitative analysis of Au-NP@SiO_x NWs structure is presented by Gentile et al. [52].

Metal oxide semiconductors (MOSs), such as SnO_2 [53, 54] and iron oxides [55], are regarded as promising building blocks in biochemical sensing because of their sensitivity in gas sensing. Their success comes from the high surface to volume ratio and sensitive band structure dynamics in both oxidizing and reducing gasses. Embedded with NPs, the gas response performance of MOS-based gas sensors is improved. The hybrid NWs with a wrinkled γ-Fe_2O_3 outer shell and embedded Au NPs [56] exhibit excellent performance in ethanol sensing with high sensitivity and selectivity. Another NPs-decorated MOSs-based sensor [25] is presented for bio-sensing by Kim et al. from Dankook University. The sensor is fabricated by growing the ZnO NWs using hydrothermal synthesis and via the immobilization of Au NPs on the NWs. This hybrid structure sensor is especially useful for sensing prostate-specific antigen (PSA), which is a biomarker for prostate cancer detection and has a low reference level. With a sensitivity of 2.06 pg/ml in PSA detection, the hybrid sensor composed of ZnO NWs and Au NPs is expected to have broad applications in real-time label-free biosensors with high sensitivity.

Integrated Waveguide-Based Biochemical Sensors

In 2001, Dostálek et al. proposed an SPP sensor based on integrated optical waveguide structure, which consists of a channel waveguide covered with layer supporting SPPs [8]. By acquiring the normalized transmitted spectrum of two different sensing medium, variation of resonant wavelength is determined to quantify the RI of the sensing medium. This sensor shows a sensitivity of 2,100 nm/RIU. The integrated waveguide was fabricated by an ion-exchange method on a BK7 glass substrate, and the biosensor was applied in the detection of human choriogonadotropin (hCG). Another SPP sensor based on a miniaturized germanium-doped silicon dioxide waveguide has been demonstrated to show a slightly higher sensitivity (2,500 nm/RIU) [57]. This biosensor was fabricated by using a plasma-enhanced chemical vapor deposition (PECVD) method, which allows to control the RI difference between core and clad precisely. The waveguide-based biosensor works to monitor the interactions of protein A, monoclonal antibody, and avian leucosis virus. **Figure 4** [58] shows a novel planar waveguide SPP sensor based on the Otto configuration. The analyte is placed between the core and gold layer, and this configuration does not require any buffer layer, which makes the design of sensor simple. The inset figure [58] illustrates the shift in resonant wavelength for a small change in RI of analyte. The sensitivity of this sensor can then be computed and the value is 4,300 nm/RIU. Researchers have proposed several biosensors for similar structures [8, 59, 60], which requires light wave to be TM polarized since TE polarized mode cannot excite surface plasma wave. A polarization wavelength interrogation biosensor proposed by Chen et al. [27] can make both TE polarized mode, and TM polarized mode produces surface plasmonic resonance.

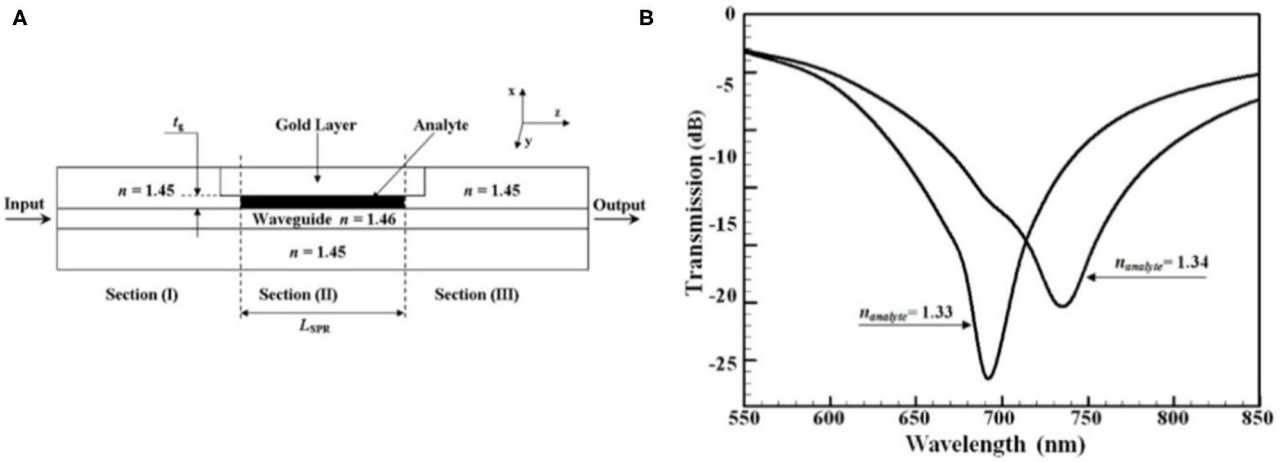

FIGURE 4 | Schematic and performance of the proposed waveguide SPP sensor [58]. **(A)** The cross section of the waveguide SPP sensor with input section (I), SPR section (II), and output section (III). **(B)** Shift in resonant wavelength with respect to $n_{analyte}$ in the proposed waveguide SPP biosensor with a 175 μm length of SPR section and a 175 nm thick analyte layer. Reprinted with permission from Akowuah et al. [58] © The Optical Society.

This biosensor was experimentally demonstrated to sense the medicine for heart disease (beta-blocker), with the sensitivity of 0.027 and 0.08 nm/ppm for TE polarized mode and TM polarized mode, respectively. The double slot hybrid plasmonic waveguide (DSHP) is an integrated waveguide made on a SiO_2 substrate by depositing Ag layer and etching part of it to create nanoscale slots. The plasmonic resonance shifts with the refractive index change of the liquid detected for estimating the presence of substances like diethyl ether ($(C_2H_5)_2O$) [16]. Also, this sensor can be used to detect the percentage of biomedical substances, such as hemoglobin in the blood of homosapiens [18]. A maximum sensitivity of 910 nm/RIU is reported.

Force and Pressure Sensors

Molecular force and pressure waves are used in various areas, including medical diagnosis, tumor ablation and geophysical exploration. To detect these physical quantities, nanostructure-based sensors are proposed. Ma et al. [61] demonstrated a nanofiber-based sensor to detect sound, which is an oscillating pressure wave. The sensor is composed of the SnO_2 nanofiber with compressible polymer cladding deposited on the surface and gold NPs decorating the fiber. Acoustic signatures, i.e., the pressure waves, can be detected by the output intensity of the transmitted light or by the scattering intensity of the individual NPs. This sensor exhibits a sensitivity $<10^{-8}$ W/m^2 under an audible frequency of 31 Hz and provides a novel method for acoustic signature analysis in miniaturized systems, such as cells or molecular machines. Based on the similar working principle, a SnO_2 nanofiber based force transducer [62] is developed with a distance sensitivity of angstrom-level and a force sensitivity of 160 fN. Researchers further used the transducer to detect sub-piconewton forces from the swimming action of bacteria with a sensitivity of −30 dB. Since the sensor has the ability to detect forces from multiple nanoparticles on a single fiber and the geometry can be inserted into small analytes, the nanofiber-based pressure sensor has great potential in biomechanical and intracellular studies.

Taking advantages of the orientational dependence of LSPR of Au nanorods (NRs), Fu et al. [63] developed a novel pressure sensor, which is a pressure-responsive polymer matrix with Au NRs embedded. Under an applied pressure, the deformation of the surrounding polymer takes place and Au NRs change their orientation, subsequently the intensity ratio of TE mode and TM mode of LSPR changes. The unique NR-based pressure sensor can be utilized for recording local distribution and magnitude of pressure and is particularly suitable for sensing in small areas with complex surface geometries.

CONCLUSION

In summary, we reviewed low-dimensional SPP sensors in this paper. **Table 1** presents the characteristics of some well-known low-dimensional plasmonic sensors. Being a label-free technique with small footprint and high sensitivity, micro- and nano-waveguide-based plasmonic sensing have been demonstrated in numerous areas, such as refractive index sensing, pressure sensing and biochemical sensing, especially. For biochemical sensing, plasmonic NW-based sensors and NPs-NWs hybrid structure based sensors are promising since their ultra-compact structure and high sensitivity for environmental changes. When it comes to the detection limit, medical diagnosis is one of the most demanding fields that require this feature, as SPP sensors with low detection limit can be applied in early detection of biomarkers. These nanosensors may probably find their applications in molecular machines and even cells systems. Another performance parameter, the dynamic range, is crucial for industrial applications, such as environmental monitoring.

Despite the high sensitivity compared to other sensing methods it acquires, the signal-to-noise ratio still needs some

TABLE 1 | Performance of low-dimensional plasmonic sensors.

Sensor configuration	Functional materials	Measured quantity	Performance	References
Fiber optic sensor	MMF coated with Ag	RI	Sensitivity of 4.5×10^{-4}∼7.5×10^{-5} RIU^{-1}	[15]
Fiber optic sensor	Ag + Si coated on fiber	RI	Sensitivity of 5.1994 μm/RIU	[38]
Waveguide based sensor	SOI rib waveguide	RI	Sensitivity of 3.968×10^4 nm/RIU	[40]
Mach-Zehnder based sensor	Waveguide coated with Au	RI	Sensitivity of 8×10^{-7} RIU/deg	[45]
Curved waveguide based sensor	GaAs waveguide surrounding by a gold ring	RI	RI resolution of 4.53×10^{-10} and dynamic range from $n = 1$ to $n = 2.36$	[46]
NW based sensor	Ag NW	NH_3	Detection limit lower than 80 ppm for NH_3	[17]
NW based sensor	Au NW	Benzene	Sensitivity of 5.5π/(μm·RIU) for 50-nm-diameter NW	[50]
NW based sensor	Pd-coated Au NW	Hydrogen	Sensitivity of ∼13 dB to 1.2% hydrogen	[20]
NP-NW hybrid sensor	Au-NPs@SiO_x NWs	O_2	The pressure of O_2 changes in the range 0∼500 Torr	[51]
NP-NW hybrid sensor	Au-NPs@γ-Fe_2O_3 NWs	Ethanol	Sensitivity of 35.1 for 50 ppm ethanol	[56]
Waveguide based sensor	Au + Cr + Ta_2O_5 coated waveguide	hCG	Detection limit of 2 ng/ml for hCG	[8]
Waveguide based sensor	Au coated waveguide	Aqueous analyte	Sensitivity of 4,300 nm/RIU	[58]
DSHP waveguide based sensor	Etched Ag coated waveguide	Hemoglobin	Sensitivity of 910 nm/RIU	[18]
DSHP waveguide based sensor	Etched Ag + Si coated waveguide	$(C_2H_5)_2O$	27.67π (nm/RIU) at the wavelength of 1,550 nm	[16]
NF based sensor	SnO_2 nanofiber	Force	Force sensitivity of 160 fN	[62]
NR based sensor	Au NRs	Pressure	Record the distribution and magnitude of pressure between two contacting surfaces	[63]

improvement due to the disturbance from the environment. Notably, the simplicity, specificity, and reliability of NW-based biochemical sensors should all be taken into account when considering the practical sensing devices. The main challenge that SPP sensors face is the high-cost platforms, which is not affordable for small research groups or communities to invest. So, the challenges of designing a portable SPP-based sensor with high sensitivity, low detection limit, broad dynamic range, low cost, and high throughput fabrication still stands out for researchers to address.

Taking an outlook of the future trend in SPP sensing, portable sensors that are user-friendly, smart, and convenient for data transmittance could be developed. Even artificial intelligence can be involved to make the signal acquisition and analysis process simpler. For biochemical sensing, the disposability of the sample container should be considered properly in fluid chip technology. Moreover, slower flow-rate and smaller sample volume in real-time detection will contribute to the promising future of biochemical sensing.

AUTHOR CONTRIBUTIONS

YL and YM organized and wrote the article. YM supervised the team. All authors discussed and participated in revising the manuscript.

FUNDING

This work was partly supported by the National Natural Science Foundation of China (61905213).

REFERENCES

1. Wijaya E, Lenaerts C, Maricot S, Hastanin J, Habraken S, Vilcot J-P, et al. Surface plasmon resonance-based biosensors: From the development of different SPR structures to novel surface functionalization strategies. *Curr Opin Solid State Mater Sci.* (2011) **15**:208–24. doi: 10.1016/j.cossms.2011.05.001
2. Chen Y, Ming H. Review of surface plasmon resonance and localized surface plasmon resonance sensor. *Photonic Sens.* (2012) **2**:37–49. doi: 10.1007/s13320-011-0051-2
3. Tong L, Xu H. Surface plasmons—mechanisms, applications and perspectives. *Physics.* (2012) **41**:582–8.
4. Nylander C, Liedberg B, Lind T. Gas detection by means of surface plasmon resonance. *Sens Actuators.* (1982) **3**:79–88. doi: 10.1016/0250-6874(82)80008-5
5. Geng Y, Wang Z, Ma Y, Gao F. Topological surface plasmon polaritons. *Acta Phys Sin.* (2019) **68**:224101. doi: 10.7498/aps.68.20191085
6. Chen L, Zhu Y, Zang X, Cai B, Li Z, Xie L, et al. Mode splitting transmission effect of surface wave excitation through a metal hole array. *Light Sci Appl.* (2013) **2**:e60. doi: 10.1038/lsa.2013.16
7. Chen L, Liao DG, Guo XG, Zhao JY, Zhu YM, Zhuang Sl. Terahertz time-domain spectroscopy and micro-cavity components for probing samples: a review. *Front Inf Technol Electron Eng.* (2019) **20**:591–607. doi: 10.1631/FITEE.1800633

8. Dostálek J, Ctyroký J, Homola J, Brynda E, Skalský M, Nekvindová P, et al. Surface plasmon resonance biosensor based on integrated optical waveguide. *Sens Actuat B Chem.* (2001) **76**:8–12. doi: 10.1016/S0925-4005(01)00559-7
9. Slavik R, Homola J, Ctyroky J, Brynda E. Novel spectral fiber optic sensor based on surface plasmon resonance. *Sens Actuat B Chem.* (2001) **74**:106–11. doi: 10.1016/S0925-4005(00)00718-8
10. Sharma A, Jha R, Gupta B. Fiber-optic sensors based on surface plasmon resonance: a comprehensive review. *IEEE Sens J.* (2007) **7**:1118–29. doi: 10.1109/JSEN.2007.897946
11. Gramotnev DK, Bozhevolnyi SI. Plasmonics beyond the diffraction limit. *Nat Photonics.* (2010) **4**:83–91. doi: 10.1038/nphoton.2009.282
12. Lee B, Roh S, Park J. Current status of micro- and nano-structured optical fiber sensors. *Opt Fiber Technol.* (2009) **15**:209–21. doi: 10.1016/j.yofte.2009.02.006
13. Jain PK, El-Sayed MA. Plasmonic coupling in noble metal nanostructures. *Chem Phys Lett.* (2010) **487**:153–64. doi: 10.1016/j.cplett.2010.01.062
14. Anker J, Hall WP, Lyandres O, Shah N, Zhao J, Duyne R. Biosensing with plasmonic nanosensors. *Nat. Mater.* (2008) **7**:442–53. doi: 10.1038/nmat2162
15. Jorgenson RC, Yee SS. A fiber-optic chemical sensor based on surface plasmon resonance. *Sens Actuat B Chem.* (1993) **12**:213–20. doi: 10.1016/0925-4005(93)80021-3
16. Singh L, Bedi A, Kumar S. Diethyl ether sensor using double nanoslot hybrid plasmonic waveguide. *Front Opt.* (2017) JTu2A.65. doi: 10.1364/FIO.2017.JTu2A.65
17. Li X, Li W, Guo X, Lou J, Tong L. All-fiber hybrid photon-plasmon circuits: integrating nanowire plasmonics with fiber optics. *Opt Express.* (2013) **21**:15698–705. doi: 10.1364/OE.21.015698
18. Lakowicz JR, Vo-Dinh T, Bedi A, Singh L, Kumar S. SPR based hybrid plasmonic waveguide sensor for detection of causes of anemia in homosapiens. *Proc SPIE.* (2018) **10509**:15. doi: 10.1117/12.2285927
19. Ricciardi A, Crescitelli A, Vaiano P, Quero G, Consales M, Pisco M, et al. Lab-on-fiber technology: a new vision for chemical and biological sensing. *Analyst.* (2015) **140**:8068–79. doi: 10.1039/C5AN01241D
20. Gu F, Zeng H, Tong L, Zhuang S. Metal single-nanowire plasmonic sensors. *Opt Lett.* (2013) **38**:1826–8. doi: 10.1364/OL.38.001826
21. Sharma P, Asad S, Ali A. Bioluminescent bioreporter for assessment of arsenic contamination in water samples of India. *J Biosci.* (2013) **38**:251–8. doi: 10.1007/s12038-013-9305-z
22. Luo B, Yan Z, Sun Z, Li J, Zhang L. Novel glucose sensor based on enzyme-immobilized 81° tilted fiber grating. *Opt Express.* (2014) **22**:30571–8. doi: 10.1364/OE.22.030571
23. Wan M, Luo P, Jin J, Xing J, Wang Z, Wong STC. Fabrication of localized surface plasmon resonance fiber probes using ionic self-assembled gold nanoparticles. *Sensors (Basel).* (2010) **10**:6477–87. doi: 10.3390/s100706477
24. Nanduri V, Bhunia AK, Tu S-I, Paoli GC, Brewster JD. SPR biosensor for the detection of L. monocytogenes using phage-displayed antibody. *Biosens Bioelectron.* (2007) **23**:248–52. doi: 10.1016/j.bios.2007.04.007
25. Kim H-M, Park J-H, Lee S-K. Fiber optic sensor based on ZnO nanowires decorated by Au nanoparticles for improved plasmonic biosensor. *Sci Rep.* (2019) **9**:15605. doi: 10.1038/s41598-019-52056-1
26. Harshita C, Rajinder SK, Balveer P. Photonic crystal waveguide-based biosensor for detection of diseases. *J. Nanophotonics.* (2016) **10**:1–10. doi: 10.1117/1.JNP.10.036011
27. Tzyy-Jiann W, Cheng-Wei T, Fu-Kun L, Hsuen-Li C. Surface plasmon resonance waveguide biosensor by bipolarization wavelength interrogation. *IEEE Photonics Technol Lett.* (2004) **16**:1715–7. doi: 10.1109/LPT.2004.828376
28. Boozer C, Kim G, Cong S, Guan H, Londergan T. Looking towards label-free biomolecular interaction analysis in a high-throughput format: a review of new surface plasmon resonance technologies. *Curr Opin Biotechnol.* (2006) **17**:400–5. doi: 10.1016/j.copbio.2006.06.012
29. Homola J. Present and future of surface plasmon resonance biosensors. *Anal Bioanal Chem.* (2003) **377**:528–39. doi: 10.1007/s00216-003-2101-0
30. *Kurabo.* (2020). Available online at: https://www.kurabo.co.jp/news/products/ (accessed July 7, 2020).
31. Ma Y, Li X, Yu H, Tong L, Gu Y, Gong Q. Direct measurement of propagation losses in silver nanowires. *Opt Lett.* (2010) **35**:1160–2. doi: 10.1364/OL.35.001160
32. Caucheteur C, Guo T, Albert J. Review of plasmonic fiber optic biochemical sensors: improving the limit of detection. *Anal Bioanal Chem.* (2015) **407**:3883–97. doi: 10.1007/s00216-014-8411-6
33. Roh S, Chung T, Lee B. Overview of the characteristics of micro- and nano-structured surface plasmon resonance sensors. *Sensors (Basel).* (2011) **11**:1565–88. doi: 10.3390/s110201565
34. Chakma S, Khalek MA, Paul BK, Ahmed K, Hasan MR, Bahar AN. Gold-coated photonic crystal fiber biosensor based on surface plasmon resonance: design and analysis. *Sens Bio-Sensing Res.* (2018) **18**:7–12. doi: 10.1016/j.sbsr.2018.02.003
35. Homola J, Piliarik M. Surface Plasmon Resonance (SPR) sensors. In: Homola J, editor. *Surface Plasmon Resonance Based Sensors*. Berlin; Heidelberg: Springer Berlin Heidelberg (2006). p. 45–67.
36. Jha R, Verma R, Gupta B. Surface plasmon resonance-based tapered fiber optic sensor: sensitivity enhancement by introducing a teflon layer between core and metal layer. *Plasmonics.* (2008) **3**:151–6. doi: 10.1007/s11468-008-9068-9
37. Monzón-Hernández D, Villatoro J. High-resolution refractive index sensing by means of a multiple-peak surface plasmon resonance optical fiber sensor. *Sens Actuat B Chem.* (2006) **115**:227–31. doi: 10.1016/j.snb.2005.09.006
38. Bhatia P, Gupta B. Surface-plasmon-resonance-based fiber-optic refractive index sensor: sensitivity enhancement. *Appl Opt.* (2011) **50**:2032–6. doi: 10.1364/AO.50.002032
39. Suzuki A, Kondoh J, Matsui Y, Shiokawa S, Suzuki K. Development of novel optical waveguide surface plasmon resonance (SPR) sensor with dual light emitting diodes. *Sens Actuat B Chem.* (2005) **106**:383–7. doi: 10.1016/j.snb.2004.08.021
40. Yuan D, Dong Y, Liu Y, Li T. Design of a high-performance micro integrated surface plasmon resonance sensor based on silicon-on-insulator rib waveguide array. *Sensors (Basel).* (2015) **15**:17313–28. doi: 10.3390/s150717313
41. Matsushita T, Nishikawa T, Yamashita H, Kishimoto J, Okuno Y. Development of new single-mode waveguide surface plasmon resonance sensor using a polymer imprint process for high-throughput fabrication and improved design flexibility. *Sens Actuat B Chem.* (2008) **129**:881–7. doi: 10.1016/j.snb.2007.09.084
42. Kabashin AV, Nikitin PI. Surface plasmon resonance interferometer for bio- and chemical-sensors. *Opt Commun.* (1998) **150**:5–8. doi: 10.1016/S0030-4018(97)00726-8
43. Nikitin PI, Beloglazov AA, Kochergin VE, Valeiko MV, Ksenevich TI. Surface plasmon resonance interferometry for biological and chemical sensing. *Sens Actuat B Chem.* (1999) **54**:43–50. doi: 10.1016/S0925-4005(98)00325-6
44. Sheridan AK, Harris RD, Bartlett PN, Wilkinson JS. Phase interrogation of an integrated optical SPR sensor. *Sens Actuat B Chem.* (2004) **97**:114–21. doi: 10.1016/j.snb.2003.08.005
45. Nemova G, Kabashin A, Kashyap R. Surface plasmon-polariton Mach-Zehnder refractive index sensor. *J Opt Soc Am B.* (2008) **25**:1673–77. doi: 10.1364/JOSAB.25.001673
46. Cheng Y-C, Chang Y-J, Chuang Y-C, Huang B-Z, Chen CC. A plasmonic refractive index sensor with an ultrabroad dynamic sensing range. *Sci Rep.* (2019) **9**:5134. doi: 10.1038/s41598-019-41353-4
47. Kim S, Yan R. Recent developments in photonic, plasmonic and hybrid nanowire waveguides. *J Mater Chem C.* (2018) **6**:11795–816. doi: 10.1039/C8TC02981D
48. Niedziółka-Jönsson J, Mackowski S. Plasmonics with metallic nanowires. *Materials (Basel).* (2019) **12**:1418. doi: 10.3390/ma12091418
49. Wei H, Zhang S, Tian X, Xu H. Highly tunable propagating surface plasmons on supported silver nanowires. *Proc Natl Acad Sci USA.* (2013) **110**:4494–9. doi: 10.1073/pnas.1217931110
50. Wang Y, Guo X, Tong L, Lou J. Modeling of Au-nanowire waveguide for plasmonic sensing in liquids. *J Lightwave Technol.* (2014) **32**:4233–8. doi: 10.1109/JLT.2014.2354696
51. Wang S-B, Huang Y-F, Chattopadhyay S, Jinn Chang S, Chen R-S, Chong C-W, et al. Surface plasmon-enhanced gas sensing in single gold-peapodded silica nanowires. *NPG Asia Mater.* (2013) **5**:e49. doi: 10.1038/am.2013.17
52. Gentile A, Ruffino F, Boninelli S, Grimaldi MG. Silica nanowire–Au nanoparticle pea-podded composites: synthesis and structural analyses. *Thin Solid Films.* (2015) **589**:755–63. doi: 10.1016/j.tsf.2015.07.011

53. Kolmakov A, Klenov DO, Lilach Y, Stemmer S, Moskovits M. Enhanced gas sensing by individual SnO2 nanowires and nanobelts functionalized with PD catalyst particles. *Nano Lett.* (2005) **5**:667–73. doi: 10.1021/nl050082v
54. Cattabiani N, Baratto C, Zappa D, Comini E, Donarelli M, Ferroni M, et al. Tin oxide nanowires decorated with Ag nanoparticles for visible light-enhanced hydrogen sensing at room temperature: bridging conductometric gas sensing and plasmon-driven catalysis. *J Phys Chem C.* (2018) **122**:5026–31. doi: 10.1021/acs.jpcc.7b09807
55. Peeters D, Barreca D, Carraro G, Comini E, Gasparotto A, Maccato C, et al. Au/ε-Fe2O3 nanocomposites as selective NO2 gas sensors. *J Phys Chem C.* (2014) **118**:11813–9. doi: 10.1021/jp5032288
56. Li N-M, Li K-M, Wang S, Yang K-Q, Zhang L-J, Chen Q, et al. Gold embedded maghemite hybrid nanowires and their gas sensing properties. *ACS Appl Mater Interfaces.* (2015) **7**:10534–40. doi: 10.1021/acsami.5b02087
57. Huang J-G, Lee C-L, Lin H-M, Chuang T-L, Wang W-S, Juang R-H, et al. A miniaturized germanium-doped silicon dioxide-based surface plasmon resonance waveguide sensor for immunoassay detection. *Biosens Bioelectron.* (2006) **22**:519–25. doi: 10.1016/j.bios.2006.07.030
58. Akowuah EK, Gorman T, Haxha S. Design and optimization of a novel surface plasmon resonance biosensor based on Otto configuration. *Opt Express.* (2009) **17**:23511–21. doi: 10.1364/OE.17.023511
59. Weiss MN, Srivastava R, Groger H. Experimental investigation of a surface plasmon-based integrated-optic humidity sensor. *Electron Lett.* (1996) **32**:842–3. doi: 10.1049/el:19960520
60. Mouvet C, Harris RD, Maciag C, Luff BJ, Wilkinson JS, Piehler J, et al. Determination of simazine in water samples by waveguide surface plasmon resonance. *Anal Chim Acta.* (1997) **338**:109–17. doi: 10.1016/S0003-2670(96)00443-6
61. Ma Y, Huang Q, Li T, Villanueva J, Nguyen NH, Friend J, et al. A local nanofiber-optic ear. *ACS Photonics.* (2016) **3**:1762–7. doi: 10.1021/acsphotonics.6b00424
62. Huang Q, Lee J, Arce FT, Yoon I, Angsantikul P, Liu J, et al. Nanofibre optic force transducers with sub-piconewton resolution via near-field plasmon–dielectric interactions. *Nat Photonics.* (2017) **11**:352–5. doi: 10.1038/nphoton.2017.74
63. Fu L, Liu Y, Wang W, Wang M, Bai Y, Chronister EL, et al. A pressure sensor based on the orientational dependence of plasmonic properties of gold nanorods. *Nanoscale.* (2015) **7**:14483–8. doi: 10.1039/C5NR03450G

Conflict of Interest: The authors declare that the research was conducted in the absence of any commercial or financial relationships that could be construed as a potential conflict of interest.